RSC Advances

PAPER

View Article Online
View Journal | View Issue

Check for updates

Cite this: *RSC Adv.*, 2026, **16**, 20117

Enhanced performance in low band gap polymer solar cells *via* surface lattice resonance of non-noble metals

Simenew A. Mulat,[ab] Fekadu G. Hone,[a] Nika Bekri *[cde] and Newayemedhin A. Tegegne *[a]

Thin-film solar cells, such as organic solar cells (OSCs), suffer from limited light absorption due to their small active-layer thickness, which is constrained by the short charge-carrier diffusion length. Plasmonic light trapping offers an effective strategy to enhance absorption without increasing the film thickness. In this work, we explore the potential of non-noble metals, namely aluminum (Al) and copper (Cu), for plasmonic enhancement in low-bandgap polymer-based OSCs and compare their performance with commonly used but costly noble metals, gold (Au) and silver (Ag), in the form of nanorods (NRs). For PTB7:$PC_{71}BM$-based OSCs, the power conversion efficiency (PCE) increases from 9.13% to 9.75% and 10.06% with Al and Cu NRs, respectively, and to 10.05% and 10.26% with Ag and Au NRs, respectively. These results indicate that a single non-noble metal NR, particularly Cu, can provide efficiency comparable to noble metals, owing to its localized surface plasmon resonance (LSPR) being closer to the absorption maximum of the active layer (AL). Furthermore, embedding NR arrays within the AL leads to a substantial enhancement in performance, with PCE improvements of 28.43% and 51.58% for Al and Cu, respectively, and 48.72% and 72.50% for Ag and Au, respectively. This enhancement is attributed to the emergence of surface lattice resonances (SLRs) arising from the hybridization of individual NR LSPRs with Rayleigh anomalies, which red-shift the plasmonic response and improve spectral overlap with the absorption of the PTB7:$PC_{71}BM$ based AL. Near-field enhancement is identified as the dominant mechanism for Au and Cu embedded devices, while far-field light scattering governs the performance improvement in Ag and Al embedded devices despite their blue-shifted LSPRs. Overall, this study highlights the strong potential of cost-effective non-noble plasmonic materials for high-performance OSCs and provides valuable insights for designing efficient light-trapping architectures.

Received 24th February 2026
Accepted 6th April 2026

DOI: 10.1039/d6ra01628f

rsc.li/rsc-advances

Open Access Article. Published on 17 April 2026. Downloaded on 4/21/2026 5:12:10 AM. This article is licensed under a Creative Commons Attribution-NonCommercial 3.0 Unported Licence.

Introduction

Organic solar cells (OSCs) are promising candidates for the next generation of green energy technologies due to their distinctive advantages, including low-cost fabrication, mechanical flexibility, lightweight design, and the possibility of roll-to-roll manufacturing of large-area devices. The power conversion efficiency (PCE) of OSCs has reached 20.6%, marking an enormous improvement over the past decade.[1] Recent advancements in the design of donor and acceptor materials, device fabrication, and characterization techniques have played key roles in the substantial improvements of OSC performance. Despite this progress, OSCs still struggle to compete with the commercially available silicon-based solar cells due to their inadequate light absorption, which is a consequence of the thin active layers (AL) (100–200 nm) constrained by the limited free charge carrier diffusion length (around 120 nm).[2] Additionally, the short exciton diffusion lengths and low charge carrier mobilities remain key limitations that need to be addressed to further improve the performance of OSCs and facilitate their commercialization.[3]

Several mechanisms have been developed to address the above-mentioned bottlenecks and enhance light absorption in thin-film OSCs. These include the use of diffraction gratings[4] and the incorporation of optical spacer layers, which can maximize the internal electromagnetic field distribution in the photoactive layer through constructive interference of the waves in the layer.[5] Furthermore, using plasmonic metallic nanostructures (PMNSs) is a promising approach for improving the PCE of OSCs.[6] In this regard, PMNSs with different shapes,[7–9]

[a]*Department of Physics, Addis Ababa University, 1176 Addis Ababa, Ethiopia. E-mail: newaye.medhin@aau.edu.et*

[b]*Department of Physics, Hawassa University, 05 Hawassa, Ethiopia*

[c]*Sustainable Energy Center of Excellence, Addis Ababa Science and Technology University, Addis Ababa, 16417, Ethiopia*

[d]*Nuclear Reactor Technology Center of Excellence, Addis Ababa Science and Technology University, Addis Ababa, 16417, Ethiopia*

[e]*Department of Mathematics, Physics and Statistics, Addis Ababa Science and Technology University, Addis Ababa, 16417, Ethiopia. E-mail: nika.bekri@aastu.edu.et*

© 2026 The Author(s). Published by the Royal Society of Chemistry

Open Access Article. Published on 17 April 2026. Downloaded on 4/21/2026 5:12:10 AM. This article is licensed under a Creative Commons Attribution-NonCommercial 3.0 Unported Licence.

photonic crystals, photonic waveguide mode, and plasmon cavity,[10] plasmonic arrays, and quantum dots have been used to effectively increase light absorption in OSC devices without increasing the physical thickness of the AL.[11] PMNSs utilize localized surface plasmonic resonance (LSPR) effects arising from their interaction with incident light to effectively amplify the local electromagnetic field and/or increase the optical path length of light within the AL of OSC devices. This enhancement occurs without altering the physical thickness of the photoactive layer, thereby increasing light absorption.[12–14]

Currently, noble metals such as gold (Au) and silver (Ag) are the primary plasmonic materials utilized to enhance the efficiency of OSCs and the most investigated in OSC research.[7,14] This is due to their pronounced LSPR effects, which contribute to the improved performance of these devices.[7]

Furthermore, mixed noble metal systems, including Ag–Au alloys, core–shell structures, and other hybrid noble PMNS architectures, have also been employed to further improve light trapping by broadening the LSPR response, thereby enabling the harvesting of a larger portion of the solar spectrum.[7,14–17] For instance, Zhao *et al.*[17] reported a PCE enhancement from 15.46 to 16.62% in PM6:Y6-based OSCs by incorporating a blend of Au nano bipyramids and nanospheres. Similarly, Phengdaam *et al.*[7] achieved a 7.9% enhancement in PCE in P3HT:PCBM-based OSCs by incorporating a mixture of Ag nano prisms into the hole transport layer (HTL), thereby enhancing light absorption through multi-mode plasmonic coupling. Prasetio *et al.*[18] also reported that Ag@SiO_2@Au NPs enhance light absorption and charge generation *via* dual plasmonic effects, improving the PCE from 7.36% to 8.57%. Furthermore, Alkhalayfeh *et al.*[19] demonstrated a ≈70% PCE improvement through LSPR-enhanced absorption upon incorporation of Au@Ag NPs into both the buffer layer and AL of PTB7:PC_{71}BM based OSCs.

Despite the excellent plasmonic performance of noble metals such as Au and Ag, their high cost and scarcity make them less suitable for large-scale applications. Consequently, there is an immediate need to explore cost-effective non-noble metal alternatives such as Cu and Al.[20,21] Both Al and Cu have recently attracted considerable attention for plasmonic applications due to their high abundance in nature and tunable plasmonic response in the UV-visible light wavelength region.[20,22–26] Moreover, their self-limiting native oxide layer can provide slight surface passivation and stability, causing only minimal changes to plasmonic modes and optical resonance.[26–29]

A number of studies have demonstrated the effective integration of Cu and Al NPs in OSCs to improve the device's performance through LSPR. For instance, Liu *et al.*[23] reported a PCE increase from 3.58% to 3.96% and from 6.79% to 7.43% by incorporating Cu NPs into the AL of P3HT:PCBM and PTB7:PCBM-based OSC devices, respectively. Seimela and coworkers[30] in their study, also reported a PCE increase from 3.93% to 5.56% by embedding Cu NRs into the PEDOT:PSS (HTL) of P3HT:PCBM-based OSCs. Krassas *et al.*[24] reported 8.7% PCE enhancement by adding Al NP in the HTL, while Yang *et al.*[31] and Ismail *et al.*[25] demonstrated that incorporating Al NPs into the AL of P3HT:PC_{60}BM-based devices can result in 29% and 39% PCE enhancements, respectively. These enhancements are primarily attributed to LSPR effects that facilitate the harvesting of photon energy and improve PCE.

The effective enhancement of photon absorption within the AL of OSCs through LSPR depends strongly on the size, shape, the refractive index of the surrounding medium, and the type of metal NPs.[32] Optimal spectral matching between the LSPR peak of the NPs and the absorption band of the photoactive layer is essential for maximizing photon absorption and hence enhancing device performance.[33,34] In this regard, different NPs of noble (Ag, Au), non-noble (Cu, and Al) have been investigated for different optoelectronic applications, demonstrating significant enhancement in J_{sc} and PCE.[21,22,35] However, comparative studies of these plasmonic NRs and their impact on OSC performance remain limited. Additionally, most reports focus on the LSPR response of individual NPs, often overlooking inter-particle interactions among NPs and their interactions with the surrounding polymer medium, which can lead to collective plasmonic–photonic coupling and enhanced light harvesting.

Beyond isolated plasmonic NPs, arranging PMNSs into periodic arrays induces collective optical effects.[36,37] Within these configurations, the coupling between LSPRs and the diffraction modes of the lattice resonance generates SLRs, which enhance near-field intensity, prolong plasmon lifetimes, reduce the optical loss or enhance the high-quality (Q) factor resonances, and improve light confinement.[29,36–40] While SLRs are widely studied in fields like biosensing, sensing, photocatalysis, and lasing, their application in OSCs is still in its early stages. The coupling between LSPR and lattice diffraction modes offers a promising strategy for enhancing optical absorption in photovoltaic architectures.[41] For instance, embedding Al nanosphere (NS) arrays in GaAs-based IOSCs and Au NRs arrays at the ZnO/BHJ interface of inverted PTB7-Th:PC_{71}BM-OSCs has shown efficiency gains of ≈22%.[27,42,43] Zhukovsky *et al.*[41] also showed that collective lattice resonances in periodic plasmonic Au NR-arrays enhance local field intensities and significantly increase photocurrent in GaAs-based IOSCs through SLR–LSPR coupling. However, the role of optimized periodicity in various metallic NR arrays (Ag, Al, Au, and Cu) for governing LSPR–SLR coupling and achieving broadband light harvesting in OSCs remains insufficiently explored.

In this work, we are reporting the potential of non-noble metallic NR arrays based on Al and Cu for plasmonic enhancement in OSC. The arrays are integrated within the low-band-gap polymer PTB7 (poly[[4,8-bis[(2-ethylhexyl)oxy]benzo[1,2-*b*:4,5-*b*]dithiophene-2,6-diyl][3-fluoro-2-[(2-ethylhexyl)carbonyl]thieno[3,4-*b*]thiophenediyl]]) blended with the fullerene acceptor [6,6]-phenyl-C_{71}-butyric acid methyl ester (PC_{71}BM). The PTB7:PC_{71}-BM blend was selected as the AL since PTB7 is a widely studied benchmark donor polymer for low-bandgap BHJ OSCs, enabling broad absorption across the visible to near-infrared (NIR) region.[44] This absorption profile aligns well with the red-shifted plasmonic resonances typically observed in metallic NRs and periodic arrays. The NRs were selected specifically as their anisotropic geometry supports tunable plasmon resonances

© 2026 The Author(s). Published by the Royal Society of Chemistry

Open Access Article. Published on 17 April 2026. Downloaded on 4/21/2026 5:12:10 AM.
This article is licensed under a Creative Commons Attribution-NonCommercial 3.0 Unported Licence.

extending into the NIR region.[26,45,46] In periodic arrays, NRs can also exhibit strong interparticle coupling and collective plasmonic SLR modes sensitive to array periodicity, making them ideal for studying the mechanisms of plasmon-enhanced light absorption. To this end, the performance of a non-noble-metal array is compared with that of noble-metal (Ag and Au) NR arrays employing three-dimensional finite-difference time-domain (FDTD) simulations. The results indicate substantial performance improvements compared to the reference device, with PCE increases of 28.43% and 51.58% for Al and Cu, respectively, and 48.72% and 72.50% for Ag and Au, respectively. These improvements are attributed to the emergence of SLRs arising from the hybridization of individual NR LSPRs with Rayleigh anomalies (RAs), which red-shift the plasmonic response and improve spectral overlap with the absorption of PTB7:$PC_{71}BM$ AL. The results of this study can provide a theoretical basis for experimental studies on non-noble-metallic NP-based OSCs and underscore the potential of periodic PMNSs to enhance light harvesting and device performance, thereby establishing a framework for cost-effective plasmonic designs in next-generation photovoltaics.

Numerical simulation method

The numerical simulations were performed using Ansys Lumerical FDTD software. The device geometry employed in this work follows an inverted architecture: glass/ITO (50 nm)/TiO_2 (30 nm)/PTB7:$PC_{71}BM$ (100 nm) (1 : 1.5 ratio)/MoO_3 (20 nm)/Ag (100 nm) as illustrated in Fig. 1(a). The device energetics, chemical structures of PTB7 and $PC_{71}BM$, and the multi-coefficient model (MCM)-fitted curves of the real (n) and imaginary (k) refractive indices of PTB7:$PC_{71}BM$ are shown in Fig. 1(b–d), respectively. The refractive index spectra of the device components, as well as the plasmonic NSs (Ag, Al, Au, and Cu), were obtained from refractive index data bases (CRC data)[47] and fitted using a multi-coefficient model for FDTD simulations. The MCM-fitted spectra of all layers except the AL are depicted in Fig. S1 and S2, and their electrical and optical properties are summarized in Table S1. The plasmonic response of the NRs was determined using a total-field scattered-field (TFSF) source in the wavelength range of 300 nm to 1000 nm[6] which was injected in the z-direction either in air ($n = 1$) or PTB7:$PC_{71}BM$ set to ($n = 2$).[47] The real and imaginary index spectra of the PTB7:$PC_{71}BM$ AL is illustrated in Fig. S3(a). Performance of the devices modeled as shown in Fig. 1(a) was determined by using a plane wave with a wavelength range of 300 nm to 1000 nm that was normally incident along the z-direction; perfectly matched layers (PMLs) were applied along the z-axis to fully absorb the incident light and avoid parasitic loss in the z-stack direction. Periodic boundary conditions were set along the x- and y-axes to accurately model the 2D NR array. The mesh override region with $dx = dy = dz = 1.5$ nm was used around the plasmonic nanorods (PNRs) and the AL to accurately resolve near-field electromagnetic distributions.[6] The object-defined background refractive index of the simulation region was set to 1.52. All simulations were performed at 300 K of temperature with a total simulation time of 500 fs to ensure field stabilization. Outside the refined region, a minimum global mesh step of 1 nm was used to maintain computational cost and time; a minimum mesh step was set at 0.25 nm.

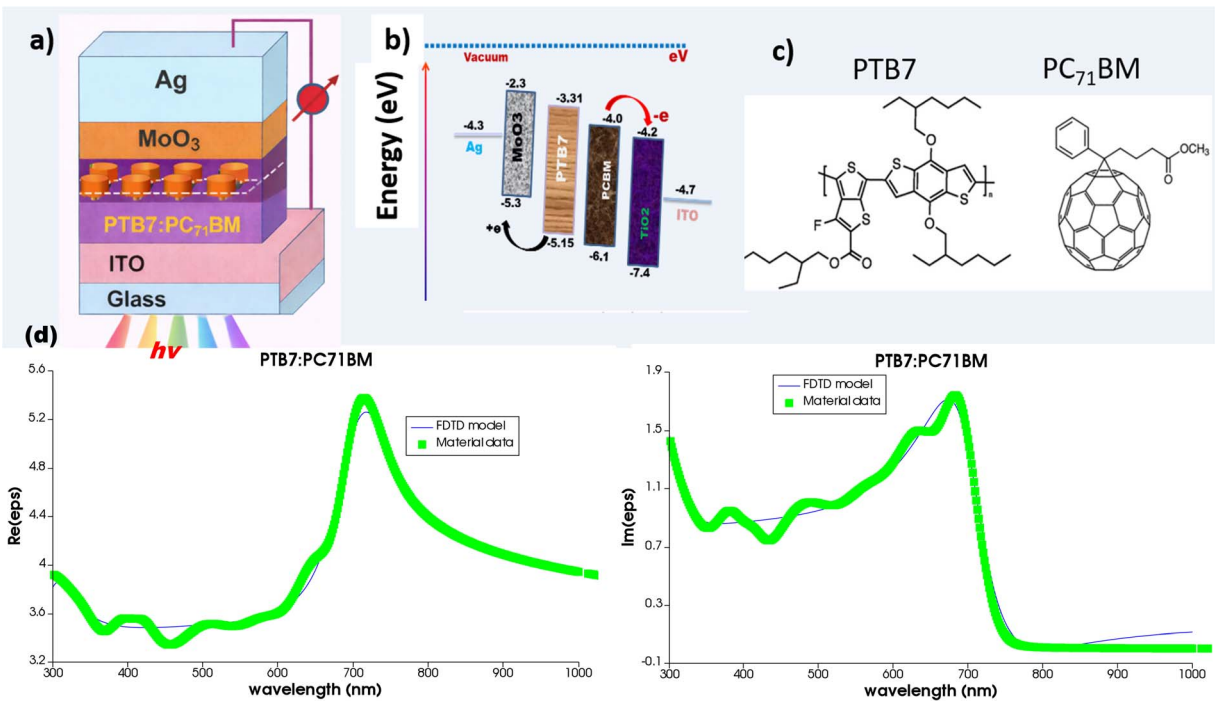

Fig. 1 (a) Device schematics of OSCs with NR-arrays embedded in (b) energetic of the device (c) chemical structures of active layer materials (d) MCM model fits for PTB7:$PC_{71}BM$ of real and imaginary parts with materials data and FDTD data.

Open Access Article. Published on 17 April 2026. Downloaded on 4/21/2026 5:12:10 AM. This article is licensed under a Creative Commons Attribution-NonCommercial 3.0 Unported Licence.

The obtained optical absorption power (P_{abs}) in the AL of OSCs was calculated using eqn (1).

$$A(\lambda) = \frac{P_{abs}(\lambda)}{P_{in}(\lambda)} \quad (1)$$

where $P_{in}(\lambda)$ is the input power.

Following this, the J_{sc} was calculated assuming an internal quantum efficiency (IQE) of 100%.[2] This assumption represents the ideal case in which an absorbed photon generates a collected electron–hole pair (exciton) and is commonly used in optical simulations to estimate the maximum theoretical photocurrent determined solely by light absorption independently of electrical losses.[2,6,48,49] The other photovoltaic parameters, V_{oc} and FF, and finally the PCE, were determined successively. Notably, in FDTD simulation, the electrical properties (V_{oc} and FF) of the OSC devices cannot be calculated directly by this simulation software, which is a limitation of this approach. Therefore, in this work, both parameters (V_{oc} and FF) are well calculated using well-established theoretical equations reported in the literature and are treated as constant values.[2,6] This assumption is justified because AL composition, charge-transport layers, and electrode materials were kept identical across all simulated configurations, whereas the embedded plasmonic nanorods primarily modify the device's optical response and light-harvesting behavior. Subsequently, the PCE was calculated using the simulated J_{sc} values together with the theoretically determined V_{oc} and FF. Detailed calculation procedures and governing equations for V_{oc}, FF, and PCE are provided in the SI (eqn (S2)–(S5)).

Results and discussion

Plasmonic properties of noble and non-noble nanorods

Plasmonic nanorods (NR) exhibit unique light–matter interactions that can be employed to enhance light harvesting in OSCs (OSCs) through their LSPR, which amplifies electromagnetic fields near the NPs surface.[6] Noble (Au and Ag) and non-noble (Cu and Al) NPs were employed in this work to explore their potential in performance enhancement of PTB7:$PC_{71}BM$-based OSCs. In this regard, the plasmonic properties of four NRs with a width of 40 nm and a length of 75 nm, namely Cu, Al, Ag, and Au, were investigated. Here, it is worth mentioning that the dimensions chosen for these calculations are based on the optimized performance (see below for details). The absorption cross-section spectra, scattering cross-section, and electric field intensity distributions of NRs were calculated using FDTD simulations in air under longitudinal light excitation, and the results are shown in Fig. 2 and S3(b). As shown in Fig. 2(a), Ag and Au NRs exhibit LSPR peaks around 390 nm and 521 nm, respectively. In contrast, Cu NR shows a broader LSPR response in the visible region, while Al displays no distinct resonance within the simulated range, indicating strong damping losses in the later.[21] These spectral variations are consistent with the differences in free-electron density, interband transitions, and dielectric properties, which collectively determine LSPR peak tunability and optical performance of the four NRs.[49] The scattering cross section of each types of PNR is also presented in Fig. S3(b). In Fig. S3(b), an Ag NR shows a more pronounced scattering cross section than the others due to its plasmonic properties.[35]

Furthermore, the electric field strength around the NRs was simulated as shown in Fig. 2(b) and the amplification factor, EFA, was determined using eqn (2).

$$\mathrm{EFA} = \frac{\iint \frac{|E(x,z)|^2}{|E_0|^2} da}{a} \quad (2)$$

where E_0 is the amplitude of the incident field, $E(x,z)$ is the induced electric field, and a is the area (a) provided in the electric field contours.

The EFA values were calculated to be 12.74, 8.26, 8.24, and 7.90 for Ag, Al, Au, and Cu, respectively. The high EFA of Ag is

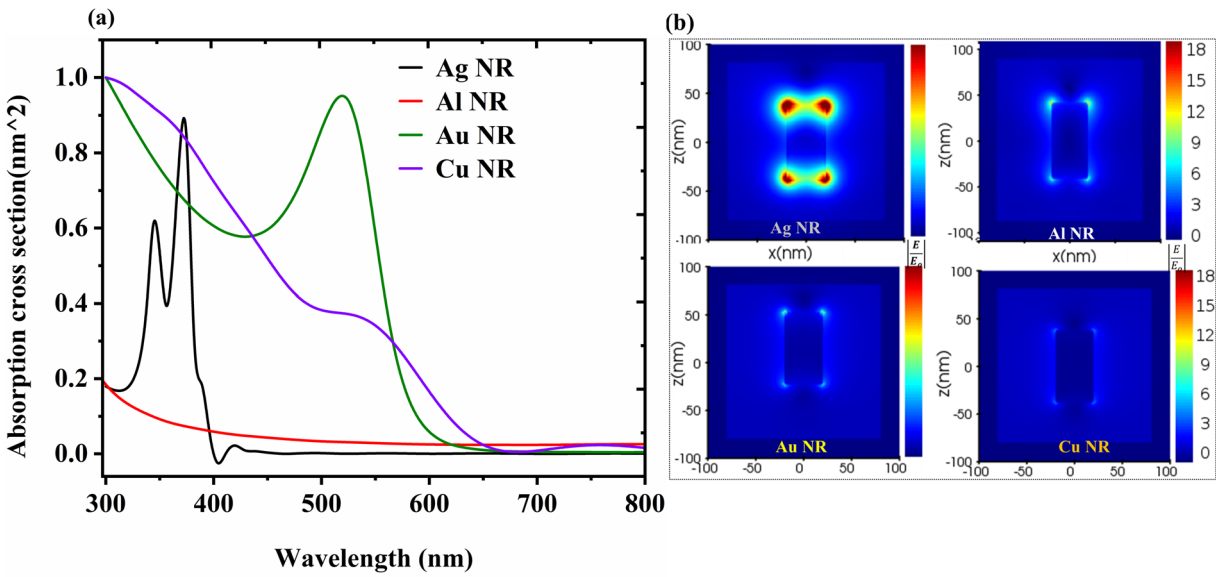

Fig. 2 (a) Absorption cross-section spectra and (b) electric field strength around Ag, Al, Au, and Cu NRs in air.

© 2026 The Author(s). Published by the Royal Society of Chemistry

Open Access Article. Published on 17 April 2026. Downloaded on 4/21/2026 5:12:10 AM. This article is licensed under a Creative Commons Attribution-NonCommercial 3.0 Unported Licence.

expected to improve light trapping when used in the AL of an OSC. It is also interesting to see that the non-noble metals, Al and Cu, also afforded comparable EFA with Au. Since light trapping using plasmonic NRs is through both their light scattering ability and EFA *via* absorbed photons, their scattering-to-absorption cross-section ratio was further calculated and found to be 0.40, 1.21, 0.10, and 0.12 in Ag, Al, Au, and Cu, respectively, indicating a much higher scattering property of Ag and Al compared to Cu and Au NRs.

In summary, it is evident that non-noble metals such as Al and Cu also show promising, comparable plasmonic performance with the most commonly used noble metals, Ag and Au. This suggests that, through appropriate tuning of their LSPR characteristics, non-noble metals can serve as cost-effective alternatives to noble metals for light harvesting in OSCs.[10,35]

Effect of aspect ratio of plasmonic nanorods on performance

It is known that the size of plasmonic NRs can be optimized to utilize the LSPR through their longitudinal and transversal modes, which can be optimized by their aspect ratios.[34] Hence, the performance of the PTB7:$PC_{71}BM$-based device was optimized by embedding NRs of different aspect ratios. The width of the NRs was kept at 40 nm for effective localized and lattice plasmonic coupling as recommended by Schmucker *et al.*[50] The aspect ratios of the NRs were changed by changing their length, and subsequently, the performance of the devices was optimized. The corresponding J_{sc} of each device with different NR of different aspect ratios is calculated using eqn (3), and following that, the PCE of the devices is calculated using eqn (S5). The calculated J_{sc} and PCE for each aspect ratio of the NRs are depicted in Fig. 3.

$$J_{sc} = q\int_{300\ nm}^{900\ nm} A(\lambda)\frac{\lambda}{hc}\mathrm{AM1.5G}(\lambda)\mathrm{d}\lambda \quad (3)$$

where AM1.5G is the solar irradiance spectrum, $A(\lambda)$ is optical absorption in the AL of the devices and is determined from the time-averaged optical absorption power in the absorber layer as estimated in eqn (1) using FDTD simulation.

The calculated J_{sc} for the pristine device was 15.36 mA cm^{-2}, yielding a device performance a PCE of 9.13%, which is in close agreement with the experimentally reported value of 9.15% for PTB7:$PC_{71}BM$-based OSCs, indicating that our simulation parameters do not overestimate the device's performance.[51] Here, it should be noted that the present calculations assume ideal device conditions with an IQE of 100%, which is commonly adopted in optical simulations to evaluate the upper limit of photocurrent generation. Nevertheless, the predicted performance remains consistent with experimentally reported values. For example, Ng *et al.* demonstrated that incorporating Au NPs into the HTL of the same PTB7:$PC_{71}BM$-based AL increased the PCE from 7.5% to 8.2%.[52] Furthermore, the obtained results are comparable to the numerical study reported by Alahmadi,[53] where a J_{sc} of 16.43 mA cm^{-2} and a PCE slightly above 8% were achieved. These comparisons confirm that the simulated device performance is near the realistic range reported in both experimental and theoretical studies. Furthermore, the calculated PCE value aligns well with the experimental study by Zhihai Liu *et al.*[23] on PTB7:$PC_{70}BM$-based conventional OSC, in which Cu NPs were incorporated into the HTL. The resulting plasmonic OSC showed an enhancement in PCE from 6.79% to 7.43%, providing strong experimental evidence for the potential of plasmonic effects of non-noble metals in OSCs. The aspect ratio of all NRs that afforded the highest J_{sc} was found to be 1.88, as shown in Fig. 3. The longitudinal LSPR of the NRs is expected to play the major role in improving the performance of the devices, as it is closer to the absorption peak of PTB7. On the contrary, the transverse mode of the NRs LSPR falls on the UV region,[54] which limits its contribution to the photon harvest of the devices. The aspect ratio is expected to tune the magnitude of both the longitudinal and transverse modes; hence, the optimization yields the highest LSPR to improve the J_{sc} and PCE of the devices. An optimized aspect ratio of plasmonic NR helps to use near-field and light-scattering enhancement charge generation in the AL of the devices, potentially improving the (J_{sc}) and (PCE).[34] Consistent with this observation, Phengdaam *et al.*[11] also reported that variations in the aspect ratio of NRs affect the tunability of the LSPR mode, thereby influencing the photovoltaic performance of OSC devices.

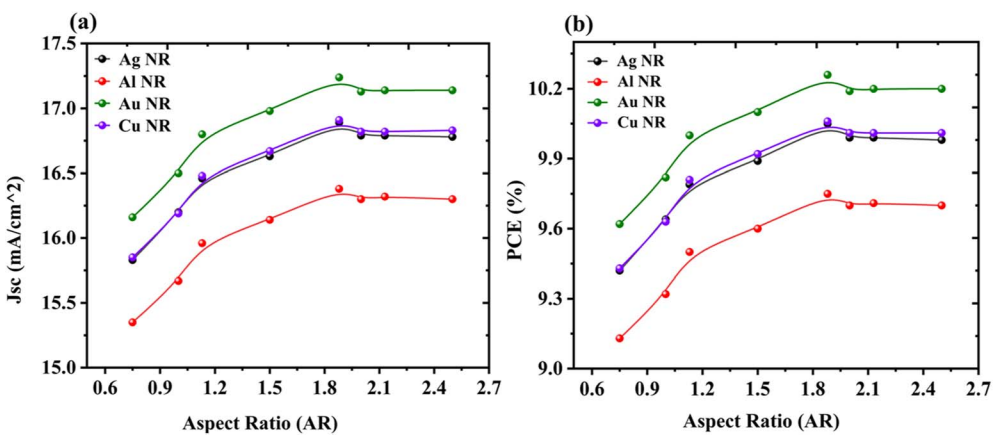

Fig. 3 (a) J_{sc} and (b) PCE of PTB7:$PC_{71}BM$-based OSCs incorporating Ag, Al, Au, and Cu NRs calculated for different aspect ratios of NRs.

Open Access Article. Published on 17 April 2026. Downloaded on 4/21/2026 5:12:10 AM.
This article is licensed under a Creative Commons Attribution-NonCommercial 3.0 Unported Licence.

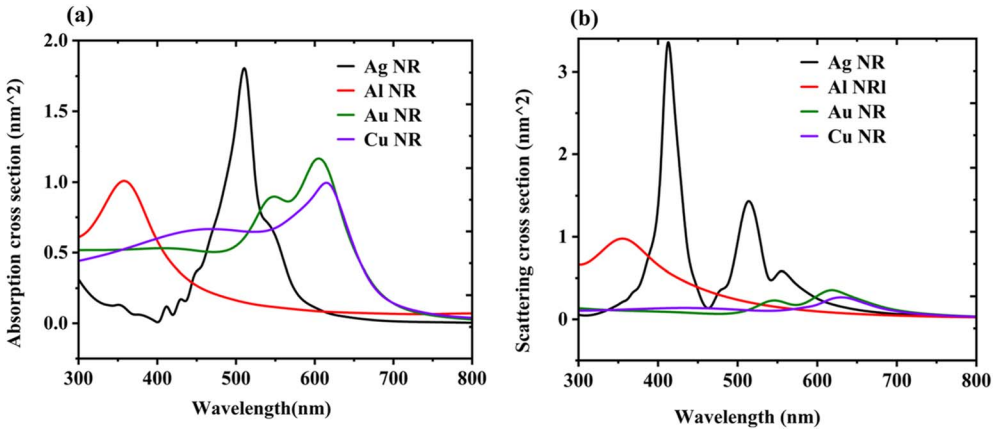

Fig. 4 (a) absorption and (b) scattering cross-sections of single NRs with an aspect ratio of 1.88 inside the active layer.

The maximum J_{sc} values obtained in Ag, Al, Au, and Cu were 16.89, 16.38, 17.24, and 16.91 mA cm^{-2}, respectively, indicating a 9.83%, 6.51%, 12.11%, and 9.96% corresponding improvement compared to the pristine device, respectively. Comparing the four NRs, it can be seen that Au afforded the highest PCE owing to its red-shifted longitudinal LSPR, while Al afforded the lowest improvement in PCE due to its UV-lying LSPR properties. It is worth mentioning that Cu produced a better improvement than Ag and a closer value to Au, despite its much lower cost compared to the noble metals, confirming the potential of non-noble metals for light trapping in OSCs. As summarized in Table 1, the performance enhancement of PTB7:$PC_{71}BM$-based OSC devices clearly shows that low-cost, non-noble metals such as Cu and Al exhibit comparable performance to noble metals and provide a benchmark for comparing noble-metal plasmonic with non-noble metals with further modification of their plasmonic effect in addition to LSPR. Furthermore, the absorption power spectra of the PTB7:$PC_{71}BM$ incorporated with Ag, Al, Au, and Cu NR of aspect ratio (1.88) is presented in Fig. S4(a) and the corresponding *J–V* curves of the devices was calculated using eqn (4) and depicted in Fig. S4(b).

Light trapping by single nanorods

The improved device performance upon embedding plasmonic NRs is primarily attributed to enhanced light trapping arising from their absorption and scattering capabilities, which together increase the effective interaction of incident photons with the AL.[20,34] To elucidate the contribution of individual plasmonic materials, the absorption and scattering cross-sections of Ag, Au, Al, and Cu NRs with an optimized aspect ratio of 1.88 embedded in the PTB7:$PC_{71}BM$ AL were calculated, as shown in Fig. 4. The absorption spectra exhibit distinct resonance peaks at approximately 500 nm for Ag, in the 600–700 nm range for Au and Cu, and below 400 nm for Al NRs. In terms of scattering, Ag and Al NRs exhibit appreciable scattering cross-sections, indicating strong plasmonic excitation accompanied by efficient collective electron oscillations and pronounced far-field scattering.

When compared with the absorption spectrum of PTB7:$PC_{71}BM$ (Fig. 1(d)), the absorption resonances of Au and Cu NRs show good spectral overlap with the photoactive layer, suggesting that their performance enhancement is dominated by near-field-mediated absorption rather than scattering. In contrast, Ag NRs exhibit both significant absorption and scattering cross-sections in a spectral region close to the AL absorption peak. The strong scattering response of Ag NRs is expected to promote light redirection and in-plane scattering into the absorber, thereby extending the optical path length and improving photon harvesting efficiency.[55] Hence, this dual contribution results in a PCE enhancement of 10.08% relative to the pristine device, despite a slight blue shift with respect to the photo absorber absorption maximum.

Conversely, Al NRs exhibit both absorption and scattering resonances predominantly in the UV region, where the contribution to photocurrent generation in PTB7:$PC_{71}BM$ is minimal. As a result, Al-based devices show the lowest PCE enhancement (6.79%). These observations highlight the importance of optimizing NR material properties and resonance positions to achieve balanced light trapping, leading to enhanced photovoltaic performance. Similar conclusions have been reported by Zhao *et al.*[34] and Phengdaam *et al.*,[7] confirming that optimized plasmonic effects can simultaneously enhance J_{sc} and PCE, consistent with the results summarized in Table 1.

To further quantify light-trapping effects induced by individual NRs, the near-field electric-field enhancement within the device was evaluated, as shown in Fig. 5. The maximum electric-

Table 1 Optimized PCE and J_{sc} of NRs embedded PTB7:$PC_{71}BM$-based OSCs

NR	J_{sc} (mA cm^{-2})	PCE (%)	$J_{sc}{}^{a}$ (%)	PCE^{a} (%)
Ag	16.89	10.05	9.83	10.08
Al	16.38	9.75	6.51	6.79
Au	17.24	10.26	12.12	12.38
Cu	16.91	10.06	9.96	10.19

[a] Enhancement relative to the reference device with J_{sc} = 15.38 mA cm^{-2} and PCE = 9.13%.

© 2026 The Author(s). Published by the Royal Society of Chemistry

Open Access Article. Published on 17 April 2026. Downloaded on 4/21/2026 5:12:10 AM.
This article is licensed under a Creative Commons Attribution-NonCommercial 3.0 Unported Licence.

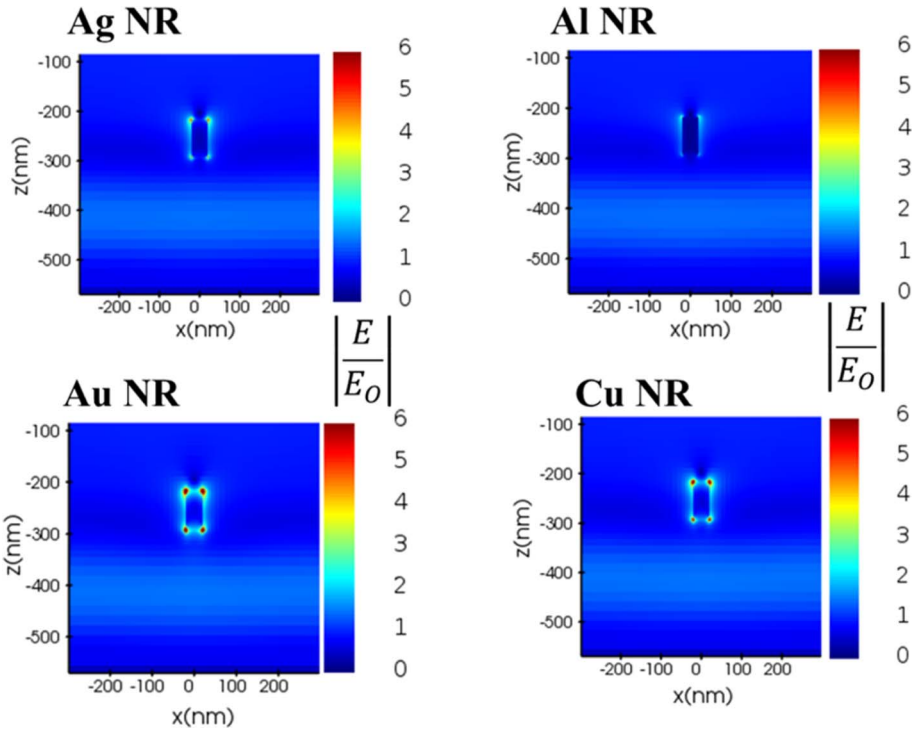

Fig. 5 Normalized electric field strength at the wavelength of 750 nm of the single NR (Ag, Al, Au, and Cu) inside the active layer.

field intensity enhancement ($|E|/|E_0|$) at 750 nm wavelength around Ag, Al, Au, and Cu NRs was found to be 8.41, 7.70, 10.35, and 9.38, respectively. These results further confirm that near-field enhancement is more pronounced for Au and Cu NRs, whereas Ag and Al NRs exhibit comparatively weaker near-field contributions, consistent with the stronger contribution of far-field scattering mechanisms in these NRs.

This study examines the optical response of plasmonic NRs for enhanced light absorption and current density in OSCs. The predicted device's performance in this work thus represents an optical upper-limit estimation under ideal charge collection.[2] In practical OSC devices, metallic NRs also influence charge transport, recombination, and local fields, with effects that depend on their size, concentration, and distribution.[14,20,34]

Effect of surface lattice resonance of NRs on performance of OSCs

In practical applications, plasmonic NRs are typically embedded in multiple numbers as homogeneously as possible. Therefore, a periodic array of optimized NRs was incorporated into a 100 nm PTB7:$PC_{71}BM$-based AL, and their plasmonic response was systematically studied. The periodicity (P) of the array was varied from 20 to 350 nm in both the x- and y-directions (see Fig. 1). The J_{sc}, of devices incorporating NR arrays, was calculated as a function of the array periodicity, as shown in Fig. 7(a). Furthermore, the J–V curves of the devices with optimized performance when NR arrays are embedded in the AL is calculated using eqn (4) and depicted in Fig. 7(b).

$$V = \frac{nkT}{q}\ln\left(\frac{J_{sc}}{J_0}+1\right) \quad (4)$$

where V is the applied voltage, n is the diode ideality factor (1.79) for PTB7:$PC_{71}BM$,[56] k is a Boltzmann constant, T is the operating temperature ($T = 300$ K), and J_0 (18.6 mA cm^{-2}) is the saturation current.[51] Under the working conditions, V, $= V_{oc}$, n, and J_0 were determined in the experimental work. In this case, parasitic resistances and shunt resistance are treated as ignored and infinite, respectively.[2]

As the periodicity increases from 20 to 350 nm, the calculated J_{sc} initially spikes at 30 nm and remains approximately constant over the range of 30–350 nm, followed by a pronounced enhancement and subsequent reduction. This behavior indicates the emergence of an additional collective optical resonance that contributes to enhanced photocurrent generation. Notably, the maximum J_{sc} for all NR-based devices is observed at a periodicity of 275 nm. For Al NRs, however, the J_{sc} values at periodicities of 30 nm and 275 nm are comparable.

Furthermore, the J_{sc}-periodicity dependence exhibits a plateau preceding the sharp increase at $P = 275$ nm. This feature is indicative of the onset of surface lattice resonance (SLR) formation, arising from the hybridization between the LSPR of individual NRs and the diffractive modes of the periodic array.[57] The formation of SLRs due to the periodicity is verified by calculating the optical cross section using the FDTD simulation, and the results are depicted in the SI (see Fig. S5(a–c)). Fig. S5(a–c) reveals narrow, strongly angle-dependent resonances that follow the Rayleigh anomaly condition, confirming the formation of surface lattice resonances. The emergence of

Open Access Article. Published on 17 April 2026. Downloaded on 4/21/2026 5:12:10 AM.
This article is licensed under a Creative Commons Attribution-NonCommercial 3.0 Unported Licence.

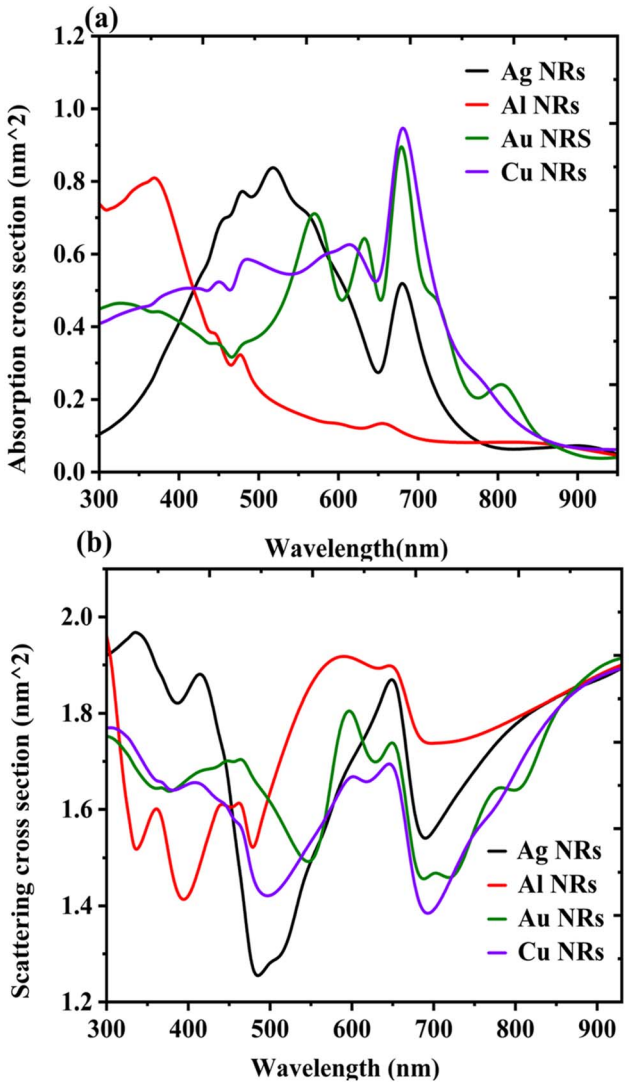

Fig. 6 (a) Absorption and (b) scattering cross-section of NR-arrays at a periodicity of 275 nm embedded in the AL.

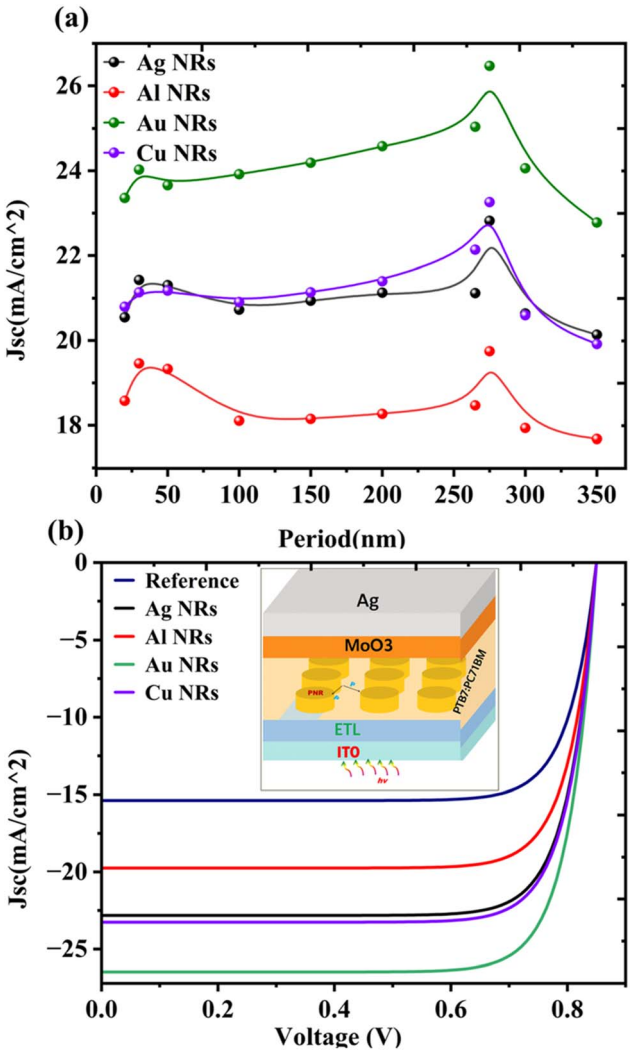

Fig. 7 J–V characteristics of OSCs incorporating NR arrays with a periodicity of 275 nm; the inset shows the device geometry.

these SLRs leads to a significant enhancement in J_{sc} compared to devices with isolated NRs, which support only localized plasmonic resonances.

The maximum J_{sc} values of the NR arrays embedded in the devices are 22.82, 19.75, 26.47, and 23.26 mA cm^{-2} for Ag, Al, Au, and Cu NRs, respectively, as given in Table 2. For single NR incorporation in the AL, the corresponding J_{sc} values are 16.89, 16.38, 17.24, and 16.91 mA cm^{-2}, while the pristine device afforded 15.36 mA cm^{-2}. Consequently, the device performance improves substantially when NR arrays are used. Correspondingly, the PCE increases when NR arrays are incorporated compared to single NRs, reaching 48.57%, 28.58%, 72.33%, and 51.43% for Ag, Al, Au, and Cu, respectively.

To elucidate the origin of the J_{sc} enhancement at a periodicity of 275 nm, we calculated the absorption and scattering cross-sections of the NRs in an array with $P = 275$ nm, as shown in Fig. 6(a) and (b), respectively. The absorption cross-sections of Ag, Au, and Cu NR arrays exhibit a sharp NIR peak compared to single NRs (Fig. 4(a)), which is absent for Al NRs. This sharp peak can be attributed to the interaction between the lattice diffraction called Rayleigh anomaly, (RA) and the NRs' LSPR, collectively forming SLRs.[36] Notably, the RA occurs approximately at $\lambda_{RA} \approx nP$, where n is the refractive index of the absorber and P is the array periodicity.[58] Hence, at high periodicities around 275 nm, λ_{RA} is sufficiently close to the LSPR of Ag, Cu, and Au NRs to enable SLR formation, whereas this is not possible for Al due to its blue-shifted LSPR. This observation is

Table 2 Optimized PCE and J_{sc} of NRs-arrays embedded PTB7:$PC_{71}BM$ based OSCs

NR	J_{sc} (mA cm^{-2})	PCE (%)	$J_{sc}{}^{a}$ (%)	PCE^{a} (%)
Ag	22.82	13.58	48.57	48.72
Al	19.75	11.75	28.58	28.43
Au	26.47	15.75	72.33	72.50
Cu	23.26	13.84	51.43	51.58

^{a} Enhancement relative to the reference device with $J_{sc} = 15.36$ mA cm^{-2} and PCE = 9.13%.

© 2026 The Author(s). Published by the Royal Society of Chemistry

Open Access Article. Published on 17 April 2026. Downloaded on 4/21/2026 5:12:10 AM.
This article is licensed under a Creative Commons Attribution-NonCommercial 3.0 Unported Licence.

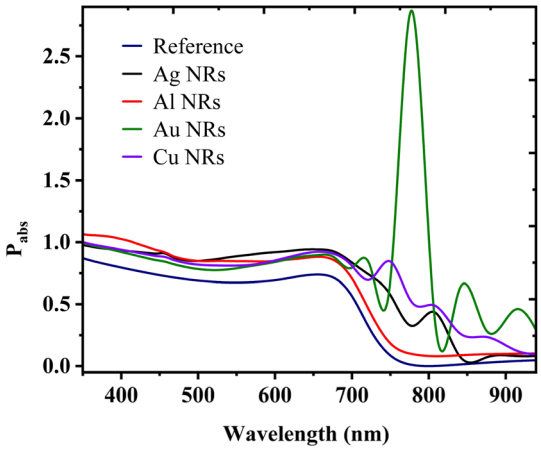

Fig. 8 Absorbed power spectra of reference and NR-array embedded OSC devices.

consistent with the maximum J_{sc} occurring at similar NR periodicities across different metals.

Light trapping *via* surface lattice resonance

As shown in Fig. 6, the incorporation of NPs arrays leads to the emergence of surface lattice resonances (SLRs), which are responsible for the improved device performance.[59] To further elucidate the differences in performance at the optimized periodicity of the NR arrays, the power absorbed spectra of devices with and without NR arrays are presented in Fig. 8.

The spectra reveal a broad enhancement in absorbed power for devices incorporating all NR arrays. However, a pronounced enhancement beyond 700 nm is observed for Au-based devices, followed successively by Cu and Ag, whereas Al does not exhibit a noticeable increase in this spectral region. Since the near-infrared (NIR) region contains significantly higher solar irradiance than the blue region, the enhanced absorption of NIR photons leads to a substantial increase in J_{sc}. This observation explains the comparatively lower J_{sc} obtained for Al-based devices.

The physical origin of the enhanced absorbed power can arise from either near-field-enhanced light absorption or far-field light scattering. To distinguish between these mechanisms, the absorbed power spectra are compared with the absorption and scattering cross-sections shown in Fig. 6. The high absorption cross-sections of Au and Cu NR arrays above 700 nm, corresponding to the SLR peak, indicate that near-field enhancement plays a dominant role in boosting photocurrent for these materials. In contrast, Ag exhibits a relatively lower absorption cross-section in this spectral region. Despite this, Ag NR array-embedded devices yield a high J_{sc}. Moreover, although Al exhibits a much lower absorption cross-section in the visible region due to the interband transition[29] an appreciable enhancement J_{sc} is still observed.

A closer examination of the scattering cross-sections in Fig. 6 reveals that Ag and Al NR arrays exhibit significantly higher scattering efficiencies. Enhanced scattering increases the optical path length of incident photons within the AL, thereby improving light trapping and absorption. Therefore, it can be concluded that the enhanced J_{sc} in Au- and Cu-based devices is primarily driven by near-field enhancement associated with SLR-mediated absorption, whereas increased far-field scattering is the dominant mechanism contributing to the photocurrent enhancement in Ag- and Al-based devices.

It is important to recognize that cu NSs (NSs) are susceptible to oxidation, forming native oxidation layers (Cu_2O or CuO) at ambient conditions.[60] As reported in the literature, the formation of these oxide layers introduces additional optical losses by modifying the dielectric function of Cu, leading to increased damping of plasmon oscillations, reduced free electron density, broadening of the LSPR, and decreased peak intensity and electric field enhancement. Furthermore, continuous oxidation results in an increase in the oxide shell thickness, which can significantly reduce or even suppress the LSPR response over time. These effects highlight the inherent limitations of Cu when compared to noble metals due to its susceptibility to oxidation for further plasmonic applications.[61,62] Despite these challenges, Cu remains a viable alternative to noble metals due to its low cost and favorable plasmonic response in the visible region. Therefore, addressing and mitigating oxidation effects are critical to successfully utilize Cu for different plasmonic applications while preserving its plasmonic properties.[63] In practical solar cell devices, this issue can be mitigated through various strategies that stabilize the Cu NPs and preserve their optical properties. One of the most common approaches is using encapsulation or protective dielectric coatings (*e.g.*, SiO_2, Al_2O_3, ZnO, or TiO_2), which have been reported to stabilize Cu plasmonic NSs while preserving their optical properties.[5,6,64,65] Polymer capping of Cu NPs is also another effective strategy to prevent the oxidation of Cu NPs and induce plasmonic near-fields that enhance the performance of SCs.[63] Cu NPs can also be positioned outside the AL, *i.e.*, within the HTL or ETL, to reduce their exposure to oxygen while still enabling plasmon-mediated light trapping through near-field coupling or back-scattering. For example, Cu nanorods embedded in PEDOT:PSS (HTL) have been reported to enhance charge transport and light harvesting in OSCs while remaining outside the AL.[30] Similarly, embedding Cu NPs within the ETL can also help in the passivation of defects, such as oxygen vacancies, while maintaining their plasmonic properties.[44] While oxidation may slightly modify the resonance characteristics, the simulations presented in this study can provide valuable insight into the intrinsic plasmonic potential of Cu NR arrays under idealized conditions. The results demonstrate their ability to enhance J_{sc} in OSCs and serve as a design guideline for experimentalists by giving a clue how stabilized Cu NSs can be employed as cost-effective plasmonic alternatives to noble metals. Although oxidation may slightly modify the resonance characteristics, the present simulations provide valuable insight into the intrinsic plasmonic potential of Cu NRs arrays under idealized conditions. The results demonstrate their ability to enhance J_{sc} in OSCs and serve as a design guideline for further experimental work. The authors wish to highlight that, with proper stabilization strategies such as dielectric coatings or encapsulation, Cu NSs can be employed as cost-effective plasmonic alternatives

Open Access Article. Published on 17 April 2026. Downloaded on 4/21/2026 5:12:10 AM.
This article is licensed under a Creative Commons Attribution-NonCommercial 3.0 Unported Licence.

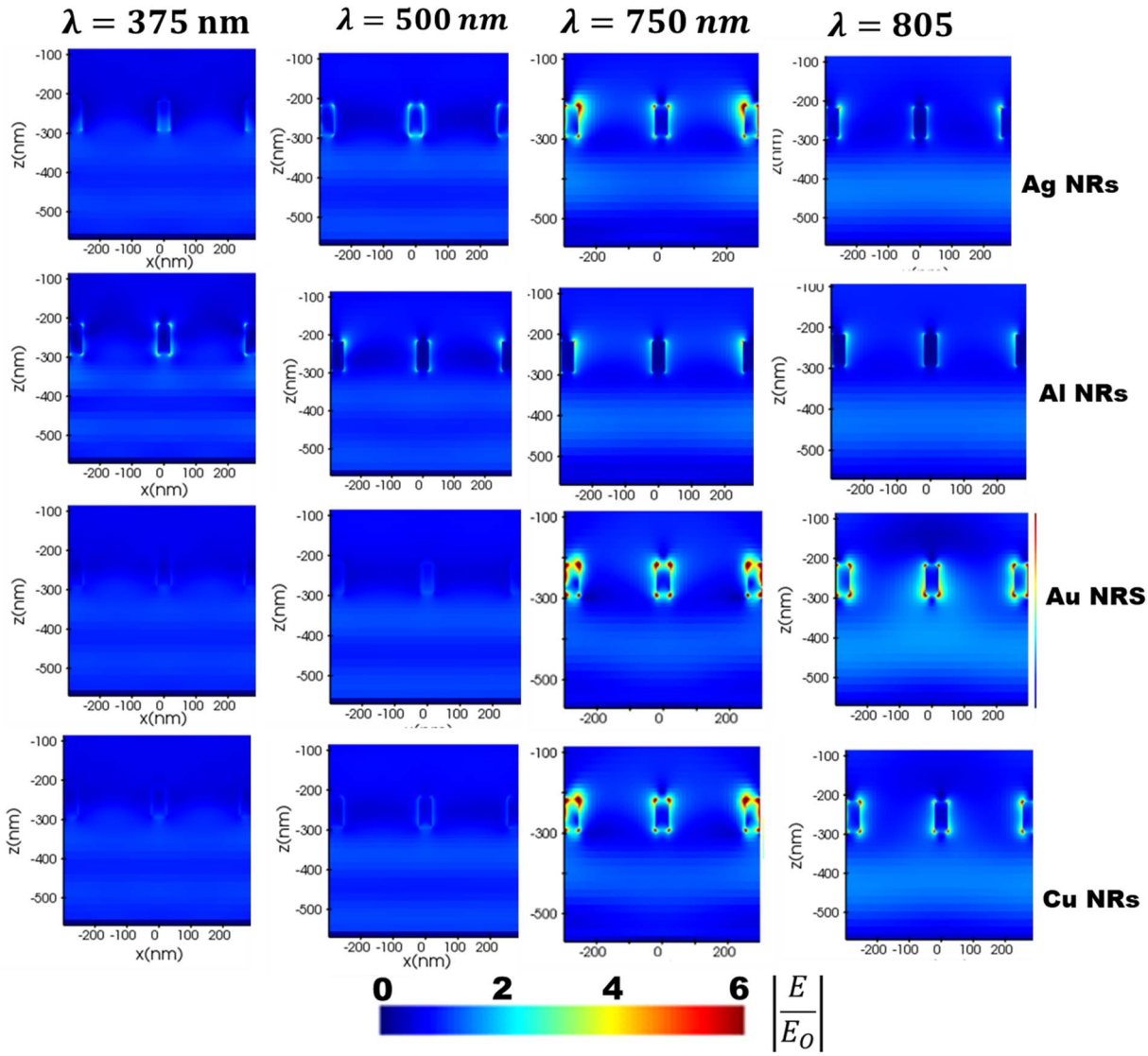

Fig. 9 Normalized electric field distribution around NR arrays calculated at different wavelengths.

to noble metals rather bare Cu NPs, bridging simulation predictions and practical devices.

Electric field amplification in OSCs with plasmonic NRs array

Leveraging plasmonic NR arrays enables collective photon scattering among neighboring NRs, which suppresses radiative losses or enhances the quality (Q) factor resonances and prolongs plasmon mode lifetimes.[29,37,66] This collective response gives rise to hybrid plasmonic–photonic modes, resulting in strong electric-field amplification within the surrounding dielectric medium.[10,58,67] Such enhanced local fields are critical for improving light harvesting and charge generation in OSC devices.

A measurable electric-field amplification is observed for all NR materials considered, as shown in Fig. 9, indicating that plasmonic enhancement is not limited to noble metals and highlighting the potential of non-noble metals in plasmonic OSC architectures. In the UV-visible region below 500 nm, Ag and Al NR arrays exhibit higher electric-field enhancement factors (E/E_0) than Au and Cu, consistent with their LSPR excitation ranges, whereas Cu and Au dominate in the region above 600 nm. At 500 nm, the E/E_0 values for Ag and Al reach 8.89 and 7.96, respectively, compared to 7.94 and 7.95 for Au and Cu. In particular, Al shows dominant enhancement in the UV region around 375 nm, as shown in Fig. 9. In contrast, at wavelengths above 600 nm, Au and Cu NR arrays exhibit significantly stronger electric-field amplification than Ag and Al. For example, at 805 nm, Ag and Al show enhancement factors of 8.69 and 8.37, respectively, whereas Au and Cu reach substantially higher values of 12.54 and 10.69. Similar plasmonic responses for Au and Cu were reported by Fabijanić *et al.*,[21] who attributed the slightly superior performance of Au to its lower intrinsic damping. Additionally, optical losses and quality factors contribute to the subtle variations in electric-field amplification observed among the plasmonic NR arrays.[37,68] The spectral region where Cu and Au showed higher electric field strength is especially relevant for PTB7:$PC_{71}BM$-based OSCs, whose absorption maximum lies above 600 nm. Consequently, the enhanced J_{sc} and

© 2026 The Author(s). Published by the Royal Society of Chemistry

Open Access Article. Published on 17 April 2026. Downloaded on 4/21/2026 5:12:10 AM.
This article is licensed under a Creative Commons Attribution-NonCommercial 3.0 Unported Licence.

PCE observed in Au- and Cu-based devices can be attributed primarily to near-field-enhanced light absorption arising from their higher electric-field amplification within the AL due to the presence of NR arrays.

Finally, a comparison of the electric field intensity distribution between periodic NR arrays and isolated single NRs at 800 nm reveals substantially stronger electric field amplification in the NR array configurations. This enhancement arises from hybrid plasmonic–photonic modes supported by the periodic NR arrangement, leading to the formation of SLRs with good quality factors.[37] These SLRs promote strong near-field coupling, enhanced far-field diffraction, and improved light localization within the AL.[29] Consequently, lattice-induced collective effects, rather than isolated plasmonic resonances alone (as discussed in the previous sections of the results and discussion), play a central role in the enhanced near-field amplification and the improved performance of NR-array-based OSC devices. It is important to note, however, that the near-field enhancement and/or far-field scattering due to the overlap of the LSPR excitation spectra with that of the AL spectra also contribute to the optical response. In this context, SLR-mediated collective effects act as the dominant mechanism, coordinating and amplifying these processes *via* coherent plasmonic–photonic coupling within the periodic array, thereby driving the observed performance enhancement. Recent studies have demonstrated that the non-radiative energy transfer mechanisms, such as plasmon-induced energy transfer (PIRET) and hot-electron injection (HEI), can occur in hybrid plasmonic systems under specific interfacial and spectral conditions.[20] However, these processes require well-defined interfacial and electronic conditions.[69]

Conclusion

The performance of low-band-gap polymer-based PTB7:$PC_{71}BM$ OSCs was enhanced by incorporating noble (Ag and Au) and non-noble (Cu and Al) plasmonic NRs (NRs). Finite-difference time-domain (FDTD) simulations were employed to systematically evaluate the optical and device performance of PTB7:$PC_{71}BM$-based OSCs with and without embedded NRs. The optimal NR aspect ratio and periodicity for maximizing light absorption and device performance were identified as 1.88 and 275 nm, respectively, for all four metallic NRs. The incorporation of a single metallic NR resulted in a 6–12.38% enhancement in PCE relative to the reference device, primarily due to LSPR. This enhancement increased to over 25% when periodic NR arrays were embedded, owing to the hybridization of LSPR with lattice diffraction, leading to the formation of surface lattice resonances (SLRs). Among the investigated NR arrays, PTB7:$PC_{71}BM$ devices incorporating Cu and Au NRs exhibited the highest PCE enhancements of 51.58% and 72.50%, respectively, compared to the reference device. These improvements are attributed to the strong spectral overlap between the hybrid plasmonic resonances and the absorption spectrum of the AL. Ag NR arrays showed a comparable enhancement of 48.72%. In contrast, devices incorporating Al NR arrays exhibited the lowest PCE improvement (28.43%), which is mainly attributed to the blue-shifted plasmonic response of Al relative to the absorption window of the PTB7:$PC_{71}BM$ AL. Mechanistically, near-field electric field enhancement was found to dominate performance improvements in Au- and Cu-based NR arrays, whereas far-field light scattering played a more significant role in Ag- and Al-based NR-embedded devices. Overall, this study demonstrates that non-noble metal NSs, particularly Cu NRs, offer a cost-effective and efficient alternative to noble metals for enhancing light harvesting, charge generation, and overall device performance in polymer solar cells, while also providing insight into mitigating oxidation effects. Furthermore, the findings provide a solid theoretical foundation for future experimental investigations of non-noble metallic nanostructure-based OSCs.

Author contributions

S. M. did all the numerical simulations work and drafted the manuscript, while N. B. and N. A. supervised and conceptualized the work. All authors contributed equally to data curation, discussion, and revision of the final manuscript.

Conflicts of interest

The authors have no conflicts of interest to declare.

Data availability

The data that support the findings of this study are available from the corresponding author upon reasonable request.

Supplementary information (SI): detailed simulation paramters, power conversion efficiency calcuations and SLR confimation plots. See DOI: https://doi.org/10.1039/d6ra01628f.

Acknowledgements

We would like to acknowledge Addis Ababa University for providing us with the simulation works facility.

References

1 J. Wang, Z. Zheng, P. Bi, Z. Chen, Y. Wang, X. Liu, S. Zhang, X. Hao, M. Zhang, Y. Li, *et al.*, Tandem organic solar cells with 20.6% efficiency enabled by reduced voltage losses, *Natl. Sci. Rev.*, 2023, **10**, nwad085.
2 P. K. Das and A. Dhawan, Plasmonic enhancement of photovoltaic characteristics of organic solar cells by employing parabola nanostructures at the back of the solar cell, *RSC Adv.*, 2023, **13**, 26780–26792.
3 K. Weng, L. Ye, L. Zhu, J. Xu, J. Zhou, X. Feng, G. Lu, S. Tan, F. Liu and Y. Sun, Optimized active layer morphology toward efficient and polymer batch insensitive organic solar cells, *Nat. Commun.*, 2020, **11**, 2855.
4 K. Hara, C. Lertvachirapaiboon, R. Ishikawa, Y. Ohdaira, K. Shinbo, K. Kato, F. Kaneko and A. Baba, Inverted organic solar cells enhanced by grating-coupled surface

Open Access Article. Published on 17 April 2026. Downloaded on 4/21/2026 5:12:10 AM. This article is licensed under a Creative Commons Attribution-NonCommercial 3.0 Unported Licence.

plasmons and waveguide modes, *Phys. Chem. Chem. Phys.*, 2017, **19**, 2791–2796.
5 K. N'konou and P. Torchio, Optical absorption enhancement by inserting ZnO optical spacer in plasmonic organic solar cells, *J. Nanophotonics*, 2018, **12**, 012502.
6 S. A. Mulat, F. G. Hone, N. Bekri and N. A. Tegegne, Improving the light harvest of plasmonic based organic solar cells by utilizing dielectric core–Shells, *Plasmonics*, 2025, **20**, 4007–4019.
7 A. Phengdaam, S. Nootchanat, R. Ishikawa, C. Lertvachirapaiboon, K. Shinbo, K. Kato, S. Ekgasit and A. Baba, Improvement of organic solar cell performance by multiple plasmonic excitations using mixed-silver nanoprisms, *J. Sci. Adv. Mater. Devices*, 2021, **6**, 264–270.
8 A. Das, K. Kumar, A. Dhawan, Plasmonics-enhanced organic solar cells with complex metallic nanoparticles, in *Photonics for Solar Energy Systems VIII*, 2020, pp 15–20.
9 M. Mohan, R. Sekar and M. A. Namboothiry, Understanding the effects of shape, material and location of incorporation of metal nanoparticles on the performance of plasmonic organic solar cells, *RSC Adv.*, 2020, **10**, 26126–26132.
10 L. Feng, M. Niu, Z. Wen and X. Hao, Recent advances of plasmonic organic solar cells: photophysical investigations, *Polymers*, 2018, **10**, 123.
11 A. Phengdaam, S. Phetsang, S. Jonai, K. Shinbo, K. Kato and A. Baba, Gold nanostructures/quantum dots for the enhanced efficiency of organic solar cells, *Nanoscale Adv.*, 2024, **6**, 3494–3512.
12 Y.-F. Li, Z.-L. Kou, J. Feng and H.-B. Sun, Plasmon-enhanced organic and perovskite solar cells with metal nanoparticles, *Nanophotonics*, 2020, **9**, 3111–3133.
13 M. A. Alkhalayfeh, A. Abdul Aziz, M. Z. Pakhuruddin and K. M. M Katubi, Spiky durianshaped Au@ Ag nanoparticles in PEDOT: PSS for improved efficiency of organic solar cells, *Materials*, 2021, **14**, 5591.
14 S. Liu, Y. Sun, L. Chen, Q. Zhang, X. Li and J. Shuai, A review on plasmonic nanostructures for efficiency enhancement of organic solar cells, *Mater. Today Phys.*, 2022, **24**, 100680.
15 M. A. Alkhalayfeh, A. A. Aziz and M. Z. Pakhuruddin, Enhancing the efficiency of polymer solar cells by embedding Au@ Ag NPs Durian shape in buffer layer, *Sol. Energy*, 2021, **214**, 565–574.
16 H. Heidarzadeh, Incorporation of plasmonic metal-metal and metal-oxide configurations in a polymer solar cell: introducing inorganic features to organic photovoltaics, *Opt. Quant. Electron.*, 2025, **57**, 244.
17 Y. Zhao, Y. Luo, S. Wu, C. Wang, N. Ahmidayi, G. Lévêque, X. Portier and T. Xu, Enhanced near-infrared photoresponse for efficient organic solar cells using hybrid plasmonic nanostructures, *Phys. E*, 2023, **146**, 115534.
18 A. Prasetio, S. Kim, M. Jahandar and D. C. Lim, Single particle dual plasmonic effect for efficient organic solar cells, *Appl. Nanosci.*, 2023, **13**, 267–273.
19 M. A. Alkhalayfeh, A. A. Aziz, M. Z. Pakhuruddin and K. M. M. Katubi, Plasmonic effects of Au@ Ag nanoparticles in buffer and active layers of polymer solar cells for efficiency enhancement, *Materials*, 2022, **15**, 5472.
20 T. Ravele, X. G. Fuku and M. A. Kebede, Review of Organic–Inorganic Heterojunction Hybrid Solar Cells with Embedded Plasmonic Nanocrystals: Recent Advances and Future Perspectives, *Energy Fuels*, 2025, **39**, 6026–6044.
21 I. Fabijanić, V. Janicki, J. Ferré-Borrull, M. Bubas, V. Blazek Bregović, L. F. Marsal and J. Sancho-Parramon, Plasmonic nanoparticles and island films for solar energy harvesting: a comparative study of Cu, Al, Ag and Au performance, *Coatings*, 2019, **9**, 382.
22 J. Katyal, others Localized surface plasmon resonance and field enhancement of Au, Ag, Al and Cu nanoparticles having isotropic and anisotropic nanostructure, *Mater. Today: Proc.*, 2021, **44**, 5012–5017.
23 Z. Liu, S. Y. Lee and E.-C. Lee, Copper nanoparticle incorporated plasmonic organic bulk-heterojunction solar cells, *Appl. Phys. Lett.*, 2014, **105**, 223306.
24 M. Krassas, G. Kakavelakis, M. Stylianakis, N. Vaenas, E. Stratakis and E. Kymakis, Efficiency enhancement of organic photovoltaic devices by embedding uncapped Al nanoparticles in the hole transport layer, *RSC Adv.*, 2015, **5**, 71704–71708.
25 Y. A. Ismail, Aluminium nanoparticles prepared by ultrasonic ablation technique inside the active layer of organic solar cell, *J. Nano Res.*, 2018, **51**, 48–60.
26 A. Zaleska, A. V. Krasavin, A. V. Zayats and W. Dickson, Copper-based core–shell metamaterials with ultra-broadband and reversible ENZ tunability, *Mater. Adv.*, 2024, **5**, 5845–5854.
27 M. M. Tharwat, A. Almalki and A. M. Mahros, Plasmon-enhanced sunlight harvesting in thinfilm solar cell by randomly distributed nanoparticle array, *Materials*, 2021, **14**, 1380.
28 P. Lv, X. Xu, W. Zhou, Q. Dong, L. Guan, Z. Li, S. Sun and L. Li, Enhancement of antimicrobial properties of plasma electrolytic oxidation coatings on aluminum alloy surfaces with CuO nanoparticles, *Ceram. Int.*, 2024, **50**, 55449–55460.
29 P. Cheng, S. Lau-Truong, S. Gam-Derouich, R. Bonnet, A. Chevillot-Biraud, M. Bräik, A. Mezeghrane, A. Belkhir, S. Li, M. Dewynter, *et al.*, Aluminum surface lattice resonances for enhanced near-infrared performance in asymmetric environments, *Nanoscale*, 2025, **17**, 21640–21648.
30 T. E. Seimela, M. S. Hamed and M. Diale, Enhancing organic solar cell performance *via* Cu nanorods-doped PEDOT: PSS: a pathway to efficient charge transport and plasmonic enhancement, *RSC Adv.*, 2025, **15**, 25929–25939.
31 S.-P. Yang, M. Yao, T. Jiang, N. Li, Y. Zhang, G. Li, X.-W. Li and G.-S. Fu, Effect of aluminium nanoparticles on the performance of bulk heterojunction organic solar cells, *Chin. Phys. Lett.*, 2012, **29**, 098402.
32 Z. Du, T. Yu, W. He, A. Yurtsever, R. Izquierdo, M. Jafari, M. Siaj and D. Ma, Enhancing efficiency of nonfullerene organic solar cells *via* using polyelectrolyte-coated plasmonic gold nanorods as rear interfacial modifiers, *ACS Appl. Mater. Interfaces*, 2022, **14**, 16185–16196.
33 O. Amargós-Reyes, A. Dzib-Chaĺe, J.-L. Maldonado and C. Arenas-Arrocena, Effect of doping the PM6: Y7 active

© 2026 The Author(s). Published by the Royal Society of Chemistry

Open Access Article. Published on 17 April 2026. Downloaded on 4/21/2026 5:12:10 AM. This article is licensed under a Creative Commons Attribution-NonCommercial 3.0 Unported Licence.

layer with MoS2 nanospheres in organic solar cells, *J. Mol. Struct.*, 2024, **1307**, 138027.
34 Y. Zhao, K. Zheng, J. Ning, T. Xu and S. Wang, Plasmonics in Organic Solar Cells: Toward Versatile Applications, *ACS Appl. Electron. Mater.*, 2023, **5**, 632–641.
35 M. Chen, Y. He, X. Wang and Y. Hu, Numerically investigating the optical properties of plasmonic metallic nanoparticles for effective solar absorption and heating, *Sol. Energy*, 2018, **161**, 17–24.
36 V. G. Kravets, A. V. Kabashin, W. L. Barnes and A. N. Grigorenko, Plasmonic surface lattice resonances: a review of properties and applications, *Chem. Rev.*, 2018, **118**, 5912–5951.
37 Q. Le-Van, E. Zoethout, E.-J. Geluk, M. Ramezani, M. Berghuis and J. Gómez Rivas, Enhanced quality factors of surface lattice resonances in plasmonic arrays of nanoparticles, *Adv. Opt. Mater.*, 2019, **7**, 1801451.
38 D. Dey and G. C. Schatz, Plasmonic surface lattice resonances in nanoparticle arrays, *MRS Bull.*, 2024, **49**, 421–430.
39 S. Hamdad, A. T. Diallo, M. Chakaroun and A. Boudrioua, The role of Rayleigh anomalies in the coupling process of plasmonic gratings and the control of the emission properties of organic molecules, *Sci. Rep.*, 2022, **12**, 3218.
40 D. Wang, J. Hu, G. C. Schatz and T. W. Odom, Superlattice surface lattice resonances in plasmonic nanoparticle arrays with patterned dielectrics, *J. Phys. Chem. Lett.*, 2023, **14**, 8525–8530.
41 S. V. Zhukovsky, V. E. Babicheva, A. V. Uskov, I. E. Protsenko and A. V. Lavrinenko, Enhanced electron photoemission by collective lattice resonances in plasmonic nanoparticle-array photodetectors and solar cells, *Plasmonics*, 2014, **9**, 283–289.
42 N. Hylton, X. Li, V. Giannini, K.-H. Lee, N. Ekins-Daukes, J. Loo, D. Vercruysse, P. Van Dorpe, H. Sodabanlu, M. Sugiyama, *et al.*, Loss mitigation in plasmonic solar cells: aluminium nanoparticles for broadband photocurrent enhancements in GaAs photodiodes, *Sci. Rep.*, 2013, **3**, 2874.
43 H. Kurt, Plasmonic enhancement in PTB7-Th: $PC_{71}BM$ organic photovoltaics, *Opt. Mater.*, 2022, **133**, 113006.
44 B. Usmani, R. Ranjan, S. K. Gupta, R. K. Gupta, K. S. Nalwa and A. Garg, others Inverted PTB7-Th: $PC_{71}BM$ organic solar cells with 11.8% PCE *via* incorporation of gold nanoparticles in ZnO electron transport layer, *Sol. Energy*, 2021, **214**, 220–230.
45 M. ul Ain, R. Ullah, Z. Fatima, A. Illahi and W. Ahmed, others Engineering gold nanoworms with tunable longitudinal plasmon peak in the near infrared and their refractive index sensing properties, *RSC Adv.*, 2024, **14**, 12772–12780.
46 A. U¸car, E. Er and G. Demirel, Anisotropic Gold Nanorod Arrays for Plasmon-Enhanced Electrochemical Sensing, *ACS Appl. Opt. Mater.*, 2024, **2**, 2551–2558.
47 M. N. Polyanskiy, Refractiveindex. info database of optical constants, *Sci. Data*, 2024, **11**, 94.
48 R. Xia, C. J. Brabec, H.-L. Yip and Y. Cao, High-throughput optical screening for efficient semitransparent organic solar cells, *Joule*, 2019, **3**, 2241–2254.
49 S. Kim, J.-M. Kim, J.-E. Park and J.-M. Nam, Nonnoble-metal-based plasmonic nanomaterials: recent advances and future perspectives, *Adv. Mater.*, 2018, **30**, 1704528.
50 A. L. Schmucker, N. Harris, M. J. Banholzer, M. G. Blaber, K. D. Osberg, G. C. Schatz and C. A. Mirkin, Correlating nanorod structure with experimentally measured and theoretically predicted surface plasmon resonance, *ACS Nano*, 2010, **4**, 5453–5463.
51 Z. He, C. Zhong, S. Su, M. Xu, H. Wu and Y. Cao, Enhanced power-conversion efficiency in polymer solar cells using an inverted device structure, *Nat. Photonics*, 2012, **6**, 591–595.
52 A. Ng, W. K. Yiu, Y. Foo, Q. Shen, A. Bejaoui, Y. Zhao, H. C. Gokkaya, A. B. Djurisic, J. A. Zapien, W. K. Chan, *et al.*, Enhanced performance of PTB7: $PC_{71}BM$ solar cells *via* different morphologies of gold nanoparticles, *ACS Appl. Mater. Interfaces*, 2014, **6**, 20676–20684.
53 A. N. Alahmadi, Design of an efficient PTB7: PC70BM-based polymer solar cell for 8% efficiency, *Polymers*, 2022, **14**, 889.
54 Y.-Y. Cai, Y. C. Choi and C. R. Kagan, Chemical and Physical Properties of Photonic Noble-Metal Nanomaterials, *Adv. Mater.*, 2023, **35**, 2108104.
55 A. G. Waketola, C. Pfukwa, P. Neethling, G. Bosman, Z. Genene, E. Wang, W. Mammo, F. G. Hone and N. A. Tegegne, Embedding plasmonic gold nanoparticles in a ZnO layer enhanced the performance of inverted organic solar cells based on an indacenodithieno [3, 2-b] thiophene-alt-5, 5-di (thiophen-2-yl)-2, 2-bithiazole-based push–pull polymer, *RSC Adv.*, 2023, **13**, 16175–16184.
56 L. Duan, H. Yi, C. Xu, M. B. Upama, M. A. Mahmud, D. Wang, F. H. Shabab and A. Uddin, Relationship between the diode ideality factor and the carrier recombination resistance in organic solar cells, *IEEE J. Photovoltaics*, 2018, **8**, 1701–1709.
57 M. Dewynter, A. Sraj, J. Loze, J. Béal, P. Cheng, K. Pandey, A. Chevillot-Biraud, N. Felidj and A.-L. Baudrion, Broadening the Plasmonic Spectral Range of Metallic Metasurfaces Using Dual-Material Arrays, *Nano Lett.*, 2026, **26**(6), 2223–2228.
58 M. S. Bin-Alam, O. Reshef, Y. Mamchur, M. Z. Alam, G. Carlow, J. Upham, B. T. Sullivan, J.-M. Ménard, M. J. Huttunen, R. W. Boyd, *et al.*, Ultra-high-Q resonances in plasmonic metasurfaces, *Nat. Commun.*, 2021, **12**, 974.
59 L. Dehbi, P. Kartikey, M. Braik, A. Belkhir, S. Lau-Truong, S. Gam-Derouich, A. Chevillot-Biraud, C. Mangeney, A. Mezeghrane, F. I. Baida, *et al.*, Tuning of plasmonic surface lattice resonances: on the crucial impact of the excitation efficiency of grazing diffraction orders, *Nanoscale*, 2025, **17**, 1536–1543.
60 Y. Fang, Z. Cheng, S. Wang, H. Hao, L. Li, S. Zhao, X. Chu and R. Zhu, Effects of oxidation on the localized surface plasmon resonance of Cu nanoparticles fabricated *via* vacuum coating, *Vacuum*, 2021, **184**, 109965.
61 Z. Liu, B. Xu, Y. Cheng, M. Si, X. Chu, M. Sun and Y. Fang, Spectral analysis of oxidation on localized surface plasmon

Open Access Article. Published on 17 April 2026. Downloaded on 4/21/2026 5:12:10 AM.
This article is licensed under a Creative Commons Attribution-NonCommercial 3.0 Unported Licence.

resonance of copper nanoparticles thin film, *Spectrochim. Acta, Part A*, 2023, **303**, 123202.

62 S. Zhao, Z. Cheng, S. Wang, H. Hao and Y. Fang, Maintaining the localized surface plasmon resonance of copper nanoparticles by defective TiO2 thin films, *Appl. Phys. A*, 2021, **127**, 930.

63 W.-J. Chen, Y.-C. Lin, G. Kumar, S.-Y. Xie and F.-C. Chen, Polymer-capped copper nanoparticles trigger plasmonic field for improving performance of perovskite solar cells, *Synth. Met.*, 2021, **273**, 116675.

64 L. Shabani, A. Mohammadi and T. Jalali, Numerical study of plasmonic effects of Ag nanoparticles embedded in the active layer on performance polymer organic solar cells, *Plasmonics*, 2022, **17**, 491–504.

65 Y. Chen, Y. Cheng and M. Sun, Physical mechanisms on plasmon-enhanced organic solar cells, *J. Phys. Chem. C*, 2021, **125**, 21301–21309.

66 D. Huang, G. Rulin, D. Qingxiu, C. Wang, Y. Li, B. Xu, D. Wu, K. Yang and H. Guan, Exciting Dark Plasmon Mode Using Heterogeneous Hybrid Cylindrical Nanostructure for SERS Detection, *Phys. Lett. A*, 2025, 130637.

67 Y. Yang, Y. Jeon, Z. Dong, J. K. Yang, M. Haddadi Moghaddam, D.-S. Kim, D. K. Oh, J. Lee, M. Hentschel, H. Giessen, *et al.*, Nanofabrication for nanophotonics, *ACS Nano*, 2025, **19**, 12491–12605.

68 B. Wang, P. Yu, W. Wang, X. Zhang, H.-C. Kuo, H. Xu and Z. M. Wang, High-Q plasmonic resonances: fundamentals and applications, *Adv. Opt. Mater.*, 2021, **9**, 2001520.

69 J. Song, J. Long, Y. Liu, Z. Xu, A. Ge, B. D. Piercy, D. A. Cullen, I. N. Ivanov, J. R. McBride, M. D. Losego, *et al.*, Highly efficient plasmon induced hot-electron transfer at Ag/TiO2 interface, *ACS Photonics*, 2021, **8**, 1497–1504.

© 2026 The Author(s). Published by the Royal Society of Chemistry